Journal of Thermal Analysis and Calorimetry (2020) 142:629–649
https://doi.org/10.1007/s10973-020-09894-3

Thermal properties and non-isothermal crystallization kinetics of biocomposites based on poly(lactic acid), rice husks and cellulose fibres

Luboš Běhálek[1] · Martin Borůvka[1] · Pavel Brdlík[1] · Jiří Habr[1] · Petr Lenfeld[1] · Dora Kroisová[2] · Filip Veselka[1] · Jan Novák[1]

Received: 2 August 2019 / Accepted: 1 June 2020 / Published online: 16 June 2020

Abstract
Bioplastics reinforced by agricultural waste fibres show promise to provide degradation back into the environment when they are no longer needed. These biocomposites have the potential to replace synthetic polymers from non-renewable resources in some applications and may turn out to be one of the material revolutions of this century. Unlike synthetic composites, biocomposites are renewable, carbon neutral, biodegradable and non-petroleum based and have low environmental, human health and safety risks. In this paper, poly(lactic acid) (PLA)-based biocomposites filled with technical cellulose fibres (CeF) and rice husks (RHs) at 10–30 mass% loading were prepared by twin-screw extrusion and injection moulding to enhance stiffness of resulting biocomposites. Particular attention was given to the enhancement of adhesion between the polymer matrix and natural filler through the physical modification by ozone (O_3) and dielectric barrier discharge (DBD) plasma (p) surface treatments. Further than, compatibilizing agent based on PLA-g-MAH was produced and introduced into the PLA systems. The non-isothermal crystallization behaviour and thermal properties were investigated through differential scanning calorimetry (DSC) under various cooling rates (5, 10, 20 and 40 °C min^{-1}). The addition of both fillers increased overall crystallization kinetics of resulted biocomposites, especially at high cooling rates. An increase in crystallinity degree from 2.4 (neat PLA) up to 51% has been observed for PLA/30CeF$_{O3}$ samples at 40 °C min^{-1} cooling rate. An increase in crystallinity degree based on mass percentage of filler was noticed especially for PLA/RH. Mass percentage increase in CeF did not notice significant increase in PLA crystallinity. The influence of RH and CeF on transformation behaviours of PLA α′-/α-polymorphs was observed. The elimination of imperfect α′-crystals was observed with increasing amount of RH and CeF.

Keywords Biocomposites · Poly(lactic acid) · Cellulose · Rice husks · Surface treatment

Introduction

Plastics are petroleum-based products that became a requisite part of our daily life in the last century. Consequently, questions about petroleum sources capacity and environmental pollution are nowadays more and more important. Therefore, many researchers and companies are focused on developed biodegradable materials made from renewable sources [1–5]. Currently, there are several common available biopolymers, among them: poly(lactic acid) (PLA); polyhydroxyalkanoate (PHA); polycaprolactone (PCL); biopolyethylene (Bio-PE); polybutylene adipate terephthalate (PBAT); and polybutylene succinate (PBS) are produced by either from bioresources or biodegradable, or both [2]. The limit of many eco-friendly materials/products consists especially in high cost and low mechanical and thermal properties [2, 6, 7].

From mentioned biopolymers, PLA has great potential to substitute petroleum-based polymers. It arises mainly due to its relatively low cost, good mechanical properties (similar to commodity plastics), biodegradability under industrial conditions and good processability. PLA is aliphatic thermoplastic polyester that is characterized by relatively high modulus and strength, excellent flavour and aroma barrier

✉ Luboš Běhálek
lubos.behalek@tul.cz

[1] Department of Engineering Technology, Faculty of Mechanical Engineering, Technical University of Liberec, Liberec, Czech Republic

[2] Department of Material Science, Faculty of Mechanical Engineering, Technical University of Liberec, Liberec, Czech Republic

properties [8]. On the other hand, it also possesses low heat deflection temperature (HDT) [6, 7], relatively high permeability to gases like water vapour or oxygen and slow crystallization rate [7, 9]. To treat these limits and enhance properties, several modifications could be made. For example, ring-opening copolymerization of lactide acid with cyclic monomers glycolide, ε-caprolactone, δ-valerolactone and trimethylene carbonate is used [1]. Blending with other polymers (e.g. PLA/PHA, PLA/PHB, PLA/MAPE, PLA/MAPP) [10] and addition of particles, additives or plasticizers are also very often used modifications [3, 11–13]. An enormous variety of natural fibres prepared form flax, hemp, straw, kenaf, jute and milling product particles from wheat, corn, soybean hulls, sorghum, oat and barely were investigated in last decades [1, 2, 14, 15]. Their thermal, physical and other properties depend not only on the applied amount and size of fibres, but also on fibres composition (e.g. content of cellulose, hemicellulose, lignin, wax and pectin) [3]. Another important parameter is adhesion between PLA and natural fibres. The cellulose-based natural fibres are generally hydrophilic, and PLA matrices are hydrophobic material with oxygen atoms [16]. This phenomenon causes poor interfacial bonding between both components. Therefore, improvement of this inherent surface incompatibility is necessary. There are several types of modifications, which could treat this problem such as chemical, biological or physical treatments. The effect of physical treatments to natural fibres consists of cleaning impurities, etching, roughening and activation of the fibre surface. It could be made via bombarding fibre surface with high-energy particles such as free radicals, ions and electrons in the plasma stream [16, 17]. In research of Jang et al. [18], a positive effect of coconut fibres plasma treatment on mechanical properties of PLA composites (increasing in tensile strength and Young's modulus) was detected. Chemical treatment is another possibility of natural fibre modification. It is not an eco-friendly method as physical treatment, but a higher impact on mechanical properties could be expected [6, 10, 19] due to mechanical interlocking reactions between cellulose –OH groups and polymer function groups. Nowadays, as commonly chemical treatment is applied, e.g. alkali treatment, silane treatment, acetylation treatment and graft copolymerization with maleic anhydrides, acrylic acid, acrylonitrile and vinyl monomers. In particular, graft copolymerization could be a very efficient way to strengthen the nonpolar polymers and natural fibres [17]. The grafted group to the side of the main chain (branched copolymers) initiates the free radicals on the cellulose molecule, which reacts with –OH bonds on the polymer matrix. Consequently, this chain interfraction adhesion improving has a positive effect on the mechanical and other material properties [17]. In publication of Bourmaund and Pimbert [20] was reported that grafted maleic anhydride on PP and PLA, which were filled with reed fibres (20, 30 and 40 mass%), increased tensile modulus by 28.6, 61.5 and 95.6%. But the tensile strength of biocomposites was without any significant changes [20]. Besides that, other chemical treatments evoke significant changes in material properties. Tran et al. [19] and Mazzanti et al. [21] reported an increase in mechanical properties and thermal stability of PLA biocomposite containing rice husk or short hemp fibres, which are modified with silane agent or alkaline treatment, respectively.

As it was mentioned above, slow crystallization kinetics and low heat deflection temperature (HDT) are other disadvantages of PLA. As a specific polymer with the stereochemical molecular composition, PLA could be produced as totally amorphous or with up to 40% crystallinity. Due to its polymorphism, PLA could crystalize in a variety of different crystal modifications [22]. Crystallization conditions during conventional injection moulding allow growth of two different polymorphs: an ordered α-phase produced at high crystallization temperatures and a disordered (condis) α′-phase that develops at low temperatures. The α′ modification has conformational disorder and a loose chain-packing manner, which defines this crystal modification as a mesophase or condis crystal. Upon slow heating in a relatively narrow temperature, region then transforms to the α-polymorph [22–25]. Conformational disorder and metastability of α′-crystals are summarized in publication of Di Lorenzo and Androsch [23]. The crystallization degree as well as crystallization rate directly depends on the macromolecular imperfections, because any imperfections decrease both parameters [1]. PLA is commonly produced as macromolecules that contain mainly L-lactide monomer and minor fraction of D-lactide groups. D-lactide induces twists in very regular PLLA architecture. Therefore, PLA with a higher content of L-lactides groups has higher crystallization ability [1]. The dependence between crystallization kinetics and molecular mass has been reported in several publications [1, 7]. The crystallization rate increases with decreasing molecular mass. Consequently, copolymerization and blending process strongly effects created morphology. Jia et al. [7] developed a special dynamic impregnating method for production of graphene oxide (GO)/polyethylene glycol (PEG) which was introduced into PLA matrix. The hybrid GO/PEG low molecular mass component enhanced crystallinity of PLA matrix, and it improved HDT properties.

With respect to the previous summary, the main aim of current studies is to enhance the limits of PLA. Hence, the objective of this study was to investigate some way of improving PLA properties. Major goal of this study was to evaluate the influence of chemical treatment based on maleic anhydride (MAH)-grafted PLA and plasma and ozone physical surface treatments of fillers on crystallization kinetics of biocomposite containing a different concentration of rice husk (RH) and cellulose fibres (CeF). The rice husk is

agriculture waste by-product, representing 23 mass% of the total production [26]. The mass composition on dry basis of rice husk has been averaged as 20 mass% ash, 22 mass% lignin, 38 mass% cellulose, 18 mass% pentosans and small amounts (2 mass%) of other organic matter [10, 27, 28]. In comparison with many renewable agriculture materials, RH has low moisture content (8%) and a considerable quantity of silica (SiO_2) [24]. Several publications, e.g. [29, 30], have been found that amorphous SiO_2, which was obtained from burning rice husk, could be used as a nucleation agent. Consequently, evaluation of the influence of physical surface plasma treatment and ozone treatment of rice husk on crystallization kinetic can reveal very interesting results. Moreover, the presence of grafted maleic anhydride in the PLA matrix can evoke some changes in the crystallization process, due to lowering molecular mass due to chains scission and enhanced adhesion. Cellulose is another easily available, renewable and fully degradable material, which could decrease product price and improve biocomposite properties. Therefore, the plasma surface modification and ozonization of cellulose-based PLA biocomposite as well as the effect of grafted maleic anhydride were evaluated.

Experimental

Materials

The commercial poly(lactic acid) (PLA) Ingeo 3001D, supplied by Nature Works (USA), was used for experimental evaluation of biocomposites non-isothermal crystallization kinetics. It is material, which contains 95 mass% of L-lactide, having approximate molecular mass 155 000, glass-transition temperature 60 °C and melting point 170 °C. The ground rice husk (RH) with average particles size 50 µm (Vietnam, Khang Ho Province) and technical cellulose fibres (CeF) purchased by Arbocel ZZC 500, J. Rettenmaier & Söhne (Germany) were applied as fillers (Fig. 1). Grinding of rice husks was made on Retsch cutting mill SM300 (Retsch, Germany). Producer of technical cellulose declares the average fibres size as a 400 µm, thickness 45 µm and chemical composition: 80–90 mass% cellulose and 10–20 mass% calcium carbonate [31]. The rice husk chemical composition is variable and depending on the type of climatic and geographical conditions, paddy, crop year and sample preparation [27].

Surface treatment of natural filler

Physical surface treatment as plasma (p) treatment and ozone (O_3) treatment was applied for improving inherent surface incompatibility between PLA matrix and used natural fillers. There are several types of plasma treatment methods [17]. The cold plasma atmospheric dielectric barrier discharge (DBD) evoked by UNIPLASMA 140 apparatus (MSV SYSTEMS CZ s.r.o, Czech Republic) was applied in this study. This apparatus is designed for continuous modification of solid or powder materials and is characterized by very high energetic efficiency (higher than commonly used plasma jet and coplanar dielectric discharge) [32]. Plasma surface treatment conditions (p) were set as follows: AC source 20 kV, AC source frequency 10 kHz, distance of electrodes: 5 mm (parallel), dielectric barrier 1: corundum, dielectric barrier 2: rubber, working gas: air (relative humidity 40%) and modification time 5 s.

The GO 5LAB (Triotech, Czech) apparatus was applied to generate ozone during surface treatments. Natural fillers (RH and CeF) were exposed to dried airflow (dew point + 5 °C, flow rate 3 L min^{-1}) with a concentration of oxygen nearly 100% and generation of ozone by 20 mg L^{-1}. Ozone concentration was measured by UV photometer LF200 (Greisinger, Germany). Elimination of redundant ozone was ensured in ozone destruction units, which is filled with active carbon. Treating time was 4 h. Additionally, the natural fillers were cleaned in pure airflow for 1 h to replace the rest of ozone.

Analysis of the surface of rice husks and cellulose fibres

The surface of rice husks and cellulose fibres was analysed using scanning electron microscopy (SEM) in a Carl Zeiss ULTRA Plus (Carl Zeiss, Germany) at an acceleration voltage range of 2–5 kV. A thin layer (several micrometers) of SiO_2 was observed on the surface of RH.

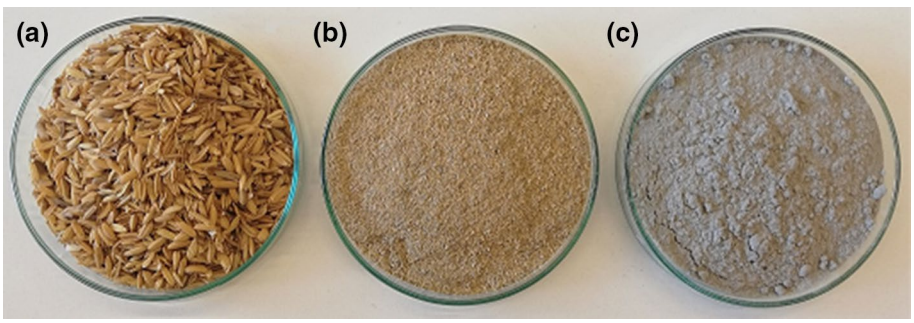

Fig. 1 Natural fillers: **a** rice husk, **b** ground rice husks, **c** cellulose fibres

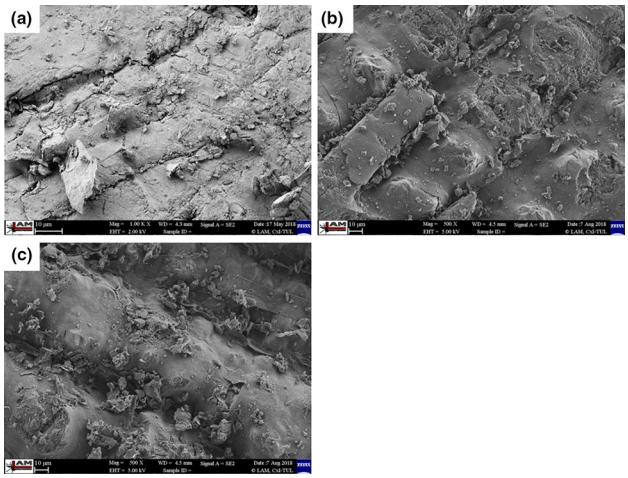

Fig. 2 SEM images of the RH surface: **a** before surface treatment, **b** after plasma modification, **c** after ozonization

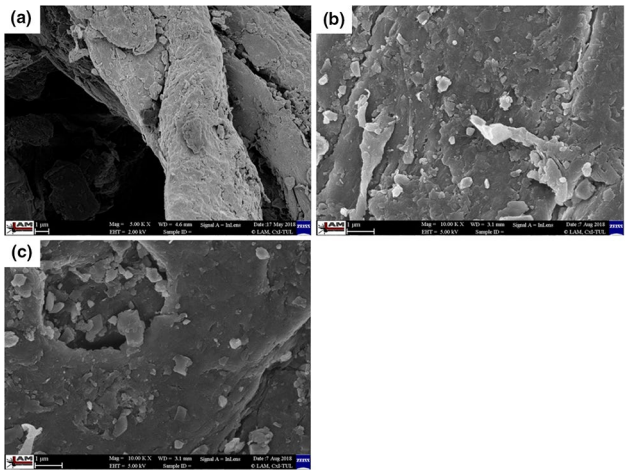

Fig. 3 SEM images of the CeF surface: **a** before surface treatment, **b** after plasma modification, **c** after ozonization

The surface of CeF is covered with small particles of $CaCO_3$ (Figs. 2 and 3).

Preparation of PLA-g-MAH

Coupling agent/interface compatibilizer composed of maleic anhydride (MAH)-grafted PLA was prepared through melt blending. PLA-g-MAH masterbatch was prepared by reactive extrusion with dicumyl peroxide (DCP) as a radical initiator. Prior to processing were PLA pellets placed in a vacuum oven and dried at 50 °C for 12 h. MAH and DCP were at first accurately weighed according to a certain ratio and dissolved in acetone. The solution was then poured into a beaker containing PLA pellets, and these were uniformly dispersed by stirring and dried in a vacuum oven to remove the solvent. The obtained mixture was then added to hopper and subjected to melt grafting reaction in a co-rotating twin-screw extruder ZK 25 E (Coolin, Germany) which was equipped with an air pelletizer EWA 10 (Econ, Austria). Processing parameters: constant temperature profile 170 °C, screw speed (100 r min^{-1}) and feed rate (30 r min^{-1}). Final concentration: PLA 94 mass%, MAH 5 mass%, DCP 1 mass%.

Preparation of biocomposites

For suitable process adjustment, the decomposition temperature of natural filler and its amount of inorganic phase were evaluated before composite production. Thermal degradation has been performed using thermal gravimetric analysis (TGA) on a TGA2 instrument (Mettler Toledo, Switzerland). Samples were heated from 50 to 600 °C under N_2 atmosphere and further from 600 to 800 °C under O_2 atmosphere at the heating ramp of 10 °C min^{-1}. The initial decomposition temperature was determined at 5% mass loss. Decomposition of rice husks takes place at 253 °C and cellulose fibres at 263 °C. The residual mass was evaluated at 800 °C. The evaluated average amount of inorganic phase (ash) of rice husk was 17 mass% and 13 mass% in cellulose fibres (Fig. 4). The chemical composition of the ash was determined by Fourier-transform infrared spectroscopy (FTIR), at ambient temperature (23 °C). FTIR spectra of rice husks, cellulose fibres and their ashes were recorded using a Nicolet iS10 FTIR spectrometer (Nicolet, USA) with deuterated lanthanum α-alanine-doped triglycine sulphate (DLaTGS) detector and diamond attenuated total reflection (ATR). In all cases, a total of 64 scans at a resolution of 4 cm^{-1} were used to record the spectra. The spectra were taken over a wavenumber range of 400–4000 cm^{-1} and were obtained with respect to a background which has been taken of the

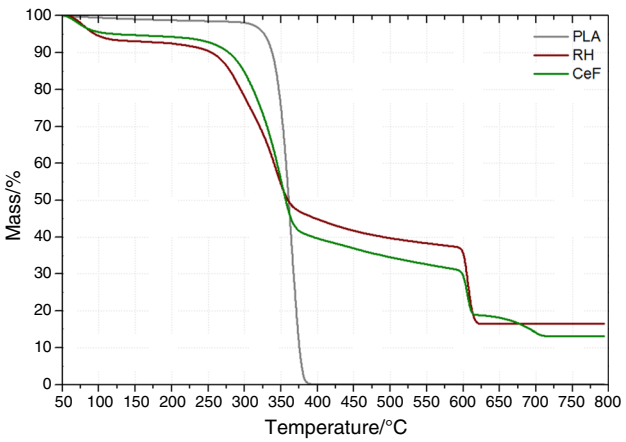

Fig. 4 TG curves of PLA, rice husks (RHs) and cellulose fibres (CeF) decomposition

air previously and under the same measurement conditions (Fig. 5). From the FTIR spectra, it can be stated that the ash of the rice husk corresponds to the majority of the silica bases minerals and the ash of the cellulose fibres to calcium carbonate. Commercial inorganic silica has peaks at 1071 cm^{-1} and 806 cm^{-1}, which can be assigned to the Si–O–Si stretching and bending vibrations [33]. The rice husk ash contained the same functional group at wavenumbers 1042 cm^{-1} and 793 cm^{-1}. On the FTIR spectrum of calcium carbonate, the fundamental bands can be seen at 708 cm^{-1} (in-plane bend), 883 cm^{-1} (out-of-plane bend) and at about 1400–1500 cm^{-1} (asymmetric stretch) [34]. The ash of technical cellulose fibres contained the same bands at wavenumbers 875 cm^{-1} and 1416 cm^{-1}. The results of ash chemical composition correspond to the results published by Cortés et al. [27] and material data sheet of Arbocel ZZC 500 [31].

Biocomposites that contain 10–30 mass% rice husk or technical cellulose (PLA/RH, PLA/CeF, PLA-g-MAH/PLA/RH and PLA-g-MAH/PLA/CeF) were prepared by co-rotation intermeshing twin-screw microcompounder MC 15 HT (Xplore, Netherlands). Microcompounder is equipped with two conical screws (172 mm mixing length and 22–9 mm cone diameters). All the biocomposite components were dried in a vacuum oven at 50 °C for 24 h. Discontinued (batch) process, at 100 r min^{-1} and 190 °C melt temperature, was applied for compounding. The advantage of this process is a uniform distribution of nature fillers, MAH, respectively, and control of the same components concentration in every test specimens. The batch homogenization to ensure sufficient dispersion of fillers was done for approximately 10 min and was followed by standard test specimen preparations by microinjection moulders IM 12 (Xplore, Netherlands). The process conditions were set as follows: 190 °C melt temperature; 35 °C mould temperature; 28-s injection and holding time (cycle time); 1.6 MPa pneumatic injection and holding pressure.

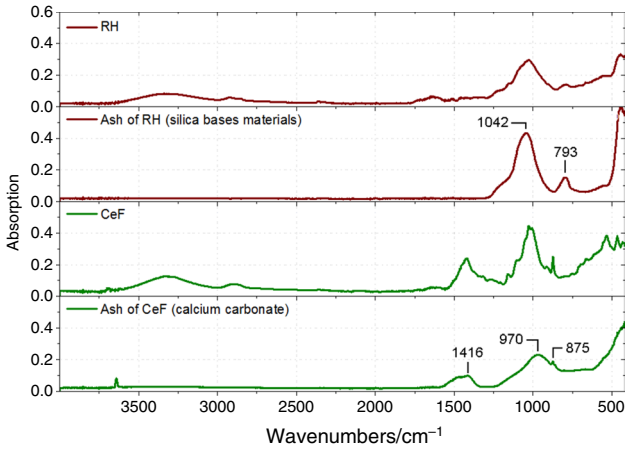

Fig. 5 FTIR spectra of rice husks (RHs) and cellulose fibres (CeF) before and after thermal decomposition: **a** RH, **b** ash of RH (silica bases minerals), **c** CeF, **d** ash of CeF (calcium carbonate)

Differential scanning calorimetry (DSC) analysis

Non-isothermal study of crystallization kinetics was performed using a DSC1/700 instrument (Mettler Toledo, Switzerland) at different cooling rates at 5 to 40 °C min^{-1}. The instrument was calibrated via indium and zinc standard. About 5–8 mg of sample was prepared from the cross section of the test specimen on a rotating microtome Leica RM2255 (Leica Biosystem, Germany) for each formulation. These were put into an aluminium pan, sealed and then placed in the DSC chamber. An empty pan was used as a reference. The experiments were performed under a constant flow of nitrogen of 50 mL min^{-1}. The samples were heated from 25 to 200 °C with heating rate 10 °C min^{-1}.

Depending on their preparation, type of filler, amount of filler and cooling rate, the following thermal properties were observed for composite systems: heat of melting (ΔH_m), heat of cold crystallization (ΔH_{cc}) and heat of premelt crystallization (ΔH_{pc}). Further, the degree of crystallinity (χ_c) was determined according to Eq. (1), where $\Delta H_m^0$is the melting enthalpy of 100% crystalline PLA (93 J g^{-1}) [2, 3] and w_m is the mass content of PLA in the composites. Unfortunately, due to a method of determination, varying values of $\Delta H_m^0$are reported in the literature [35]. Moreover, the following were tracked: melting temperature (T_m), cold crystallization temperature (T_{cc}), premelt crystallization temperature (T_{pc}), melt crystallization temperature (T_c), heat of melt (primary) crystallization (ΔH_c) and non-isothermal crystallization kinetics. Each run of specific cooling rate was determined the variation of relative crystallinity (X_T) as a function of the temperature. Relative crystallinity was calculated according to Eq. (2), where ΔH_T is the heat of melt crystallization, and T, T_0, T_∞ and H_c represent the temperature at any given moment, initial temperature, final temperature and heat of melt crystallization, respectively. Relative crystallinity at T_c (X_{Tc}) is specified in Table 3. The melt crystallization time (t_c) is given by Eq. (3), where CR is the cooling rate:

$$X_c = \frac{\Delta H_m - \Delta H_{pc} - \Delta H_{cc}}{\Delta H_m^0 \cdot w_m} \times 100\% \quad (1)$$

$$X_{Tc} = \frac{\Delta H_T}{\Delta H_c} = \frac{\int_{T_0}^{T} \left(\frac{dH_c}{dT}\right) dT}{\int_{T_0}^{T_\infty} \left(\frac{dH_c}{dT}\right) dT} \times 100\% \quad (2)$$

$$t_c = \frac{T_0 - T}{CR}. \quad (3)$$

Table 1 Thermal analysis (DSC) data for the obtained PLA composites with ground rice husks (RHs)

Sample code and mass/mg	CR/°C min^{-1}	ΔH_m/J g^{-1}	ΔH_{pc}/J g^{-1}	ΔH_{cc}/J g^{-1}	χ_c/%	$T_{m\alpha}$/°C	$T_{m\alpha}$/°C	T_{pc}/°C	T_{cc}/°C	T_c/°C	ΔH_c/J g^{-1}
PLA	5	38.64	1.18	17.63	21.3	–	168.7	153.4	107.6	95.9	12.71
5.53	10	37.09	–	32.49	4.9	163.9	169.7	–	111.9	92.7	0.93
	20	37.80	–	35.06	2.9	163.9	169.9	–	112.7	–	–
	40	37.91	–	35.67	2.4	163.9	170.1	–	112.9	–	–
PLA/10RH	5	35.90	0.37	20.51	17.9	–	168.8	153.2	110.7	96.3	7.87
6.99	10	36.15	–	31.19	5.9	163.5	170.0	–	112.1	94.6	0.40
	20	36.64	–	32.94	4.4	163.1	170.0	–	112.4	–	–
	40	36.66	–	33.69	3.5	163.3	170.0	–	112.6	–	–
PLA/20RH	5	34.66	0.77	2.24	42.5	–	167.4	154.2	97.3	98.8	23.19
7.34	10	34.14	0.57	22.16	15.3	–	167.7	155.4	103.9	93.9	2.99
	20	34.44	–	27.60	9.2	–	167.9	–	105.3	–	–
	40	34.51	–	28.38	8.2	–	168.1	–	105.4	–	–
PLA/30RH	5	31.72	–	–	48.7	–	167.9	–	–	101.0	25.74
6.96	10	32.26	1.68	14.88	24.1	–	167.6	154.2	101.0	94.3	6.6
	20	30.50	0.71	23.47	9.7	–	167.2	155.6	102.9	–	–
	40	30.68	0.37	24.16	9.4	–	167.9	155.9	103.1	–	–
PLA/10RH$_P$	5	36.31	1.38	6.89	33.5	–	168.0	153.8	102.5	98.1	20.56
5.79	10	34.57	–	25.94	10.3	162.4	168.9	–	108.7	94.2	1.62
	20	34.89	–	29.09	6.9	162.3	169.2	–	109.0	–	–
	40	34.82	–	29.79	6.0	162.3	169.2	–	109.2	–	–
PLA/20RH$_P$	5	32.39	0.7	2.64	39.0	–	168.2	153.8	100.3	99.7	22.73
5.34	10	31.81	0.6	20.55	14.3	–	168.4	154.9	104.3	95.1	4.00
	20	31.41	–	24.44	9.4	–	168.5	–	105.4	–	–
	40	31.29	–	26.77	6.1	–	168.7	–	105.6	–	–
PLA/30RH$_P$	5	29.57	0.6	1.16	42.7	–	168.0	154.3	97.0	99.2	21.56
5.73	10	29.42	0.97	18.36	15.5	–	167.9	154.8	102.7	94.1	3.86
	20	28.14	0.36	21.97	8.9	–	168.2	155.9	103.7	–	–
	40	28.02	0.35	22.40	8.1	–	168.2	155.9	103.7	–	–
PLA/10RH$_{O3}$	5	35.86	1.4	13.24	25.3	–	168.3	153.8	106.1	96.8	13.69
5.69	10	34.16	–	29.32	5.8	162.5	169.5	–	110.7	93.2	1.24
	20	35.36	–	31.70	4.4	162.0	169.7	–	111.4	–	–
	40	34.82	–	30.92	4.7	162.0	169.9	–	111.6	–	–
PLA/20RH$_{O3}$	5	31.64	1.24	3.9	35.6	–	168.3	153.4	98.1	98.0	19.10
5.58	10	31.17	1.8	18.80	14.2	–	167.7	153.6	99.2	93.7	3.15
	20	30.58	1.65	22.92	8.1	–	167.7	154.1	99.7	–	–
	40	30.64	1.59	23.07	8.0	–	167.7	154.1	99.5	–	–
PLA/30RH$_{O3}$	5	29.18	0.84	1.67	40.9	–	167.8	154.4	95.8	98.6	19.50
6.09	10	28.31	0.8	18.77	13.9	–	168.2	155.3	104.7	93.9	2.37
	20	28.13	–	22.84	8.1	–	168.5	–	105.7	–	–
	40	28.17	–	22.71	8.4	–	168.5	–	105.9	–	–
PLA-g-MAH/PLA/10RH	5	36.57	1.38	6.4	34.6	–	168.2	153.7	101.9	98.2	19.69
	10	34.95	–	27.87	8.5	162.8	169.3	–	109.4	94.1	1.51
7.28	20	35.86	–	31.05	5.8	162.8	169.4	–	109.6	–	–
	40	35.25	–	31.83	4.1	162.8	169.6	–	109.9	–	–
PLA-g-MAH/PLA/20RH	5	33.69	0.58	–	44.7	–	168.4	155.2	–	99.1	23.82
	10	33.09	0.65	21.63	14.6	–	168.6	155.2	104.5	93.3	2.47
7.40	20	33.07	–	26.46	8.9	–	168.9	–	105.7	–	–
	40	33.22	–	27.23	8.1	–	169.0	–	105.9	–	–
PLA-g-MAH/PLA/30RH	5	29.60	0.25	–	45.4	–	168.5	155.2	–	99.8	23.30
7.22	10	29.76	0.61	19.35	15.1	–	168.5	154.4	105.0	92.9	2.95

Table 1 (continued)

Sample code and mass/mg	CR/°C min^{-1}	ΔH_m/J g^{-1}	ΔH_{pc}/J g^{-1}	ΔH_{cc}/J g^{-1}	χ_c/%	$T_{m\alpha'}$/°C	$T_{m\alpha}$/°C	T_{pc}/°C	T_{cc}/°C	T_c/°C	ΔH_c/J g^{-1}
	20	30.13	–	23.50	10.2	–	168.8	–	106.1	–	–
	40	30.14	–	24.52	8.7	–	168.8	–	106.4	–	–

CR: cooling rate; RH_P: the plasma-treated surface of the rice husks; RH_{O3}: ozone-treated rice husk surface

Determination of flexural modulus

The presence of particle fillers in polymer composites as well as morphology changes (especially in surface layer of injection moulding products) has significant influence on stiffness. The stiffness of composites was evaluated by determination of flexural modulus. The three-point flexural test (according ISO 178) was made by TiraTest tensile testing machine, which is equipped with KAF type of load cells (ranging from 0 to 1000 N, sensitivity 2.0 mV/V) and with WA-type series displacement transducers (max. linearity deviation: − 0.13% and nominal supply voltage: 80 mV/V). The determination of flexural modulus was made on specimens with size 80 × 10 × 4 mm by loading rate of 2 mm min^{-1} (sampling frequency during recording: 500 Hz). This loading rate corresponds to specimen deformation rate of 1% min^{-1}. Samples were prior to testing conditioned in climatic chamber (Teseco, Czech Republic) at temperature 35 °C and 80% relative humidity for 10 days.

Results and discussion

Absolute degree of crystallinity

PLA is due to its slow crystallization rate, characteristic in heating phase with cold crystallization and sometimes also with premelt crystallization. The level of these exothermal reactions has an influence on values of heat of crystal melting. Consequently, the values of heat of cold and premelt crystallization are necessary to subtract from the heat of melting of PLA, respectively, PLA composites (Eq. 1). Evaluated heat of melting (ΔH_m), heat of cold crystallization (ΔH_{cc}), heat of premelt crystallization (ΔH_{pc}) and percentage crystallinity (χ_c) data are for PLA and PLA rice husk-based composites provided in Table 1 and for cellulose fibre-based composites in Table 2.

It is well known that the degree of crystallinity (χ_c) decreases with increasing cooling rate [36]. This decrease was for pure PLA higher than for PLA composites containing ground RH and CeF. There was observed 90% decrease in degree of crystallinity for pure PLA and 80% decrease for composites containing RH, after increasing cooling rate from 5 to 40 °C min^{-1} (Table 1). The cellulose fibre-based PLA composites evoked only 20% decrease in degree of crystallinity, at the same cooling rates (Table 2). It means that CeF has during crystallization better nucleation effect than ground RH. The degree of crystallinity increased in range from 1.6 × to 2.5 × (depending on cooling rate) when the PLA composites contain 10 mass% of RH (Fig. 6). By the same amount of CeF in PLA composites, there was detected increasing in range from 2.8 to 19 ×. The highest increase corresponds to the highest cooling rate (Fig. 7). Further, the influence of fillers amount is also obvious. By the 30 mass% of nature fillers (NFi) and the highest cooling rate of 40 °C min^{-1}, the PLA/RH degree of crystallinity increased by almost 4 × and for PLA/CeF almost 21 × (Fig. 8). It can be presumed (due to higher melt crystallization temperature and heat of melt crystallinity) that considerable increasing degree of crystallinity of PLA/CeF composites is enhanced with $CaCO_3$ presence in cellulose fibres. This statement is consistent with results research of Eiras and Pessan [37] where the nucleation effect of $CaCO_3$ nanoparticles on crystallization of PP was proved. In this study, the degree of crystallinity and the melt crystallization temperature of PP increased at addition of $CaCO_3$.

An increase in degree of crystallinity is detected with increased amount of ground RH and CeF. The highest changes were evaluated by the highest cooling rate (Tables 1 and 2). The composite containing RH reached the highest changes in variety of mass compositions under 40 °C min^{-1} cooling rate where the surface treatment was not applied. The degree of crystallinity was increased in PLA/30RH composite 2.7 × compared to PLA/10RH composite (Fig. 9). Contrariwise, the ozone surface treatment evoked the highest degree of crystallinity for cellulose-based composites. The degree of crystallinity was in PLA/30CeF_{O3} composite increased about 32% compared to PLA/10CeF_{O3} (Fig. 10). The influence of filler amount was very important, especially for RH-based composites.

The results of PLA-g-MAH introduction and plasma surface treatment of RH declare that both structure modifications have, in low filler concentrations, significant impact on degree of crystallinity. It is obvious especially at slow cooling rate. The comparable increase was observed for plasma surface treatment of PLA composites which contains 10 mass% of RH and PLA composites with grafted maleic anhydride (PLA-g-MAH/PLA/10RH). The rice husk composites without surface treatment or with ozone treatments

Table 2 Thermal analysis (DSC) data for the obtained PLA composites with cellulose fibres (CeF)

Sample code and mass/mg	CR/°C min^{-1}	ΔH_m/J g^{-1}	ΔH_{pc}/J g^{-1}	ΔH_{cc}/J g^{-1}	χ_c/%	$T_{m\alpha}$/°C	$T_{m\alpha}$/°C	T_{pc}/°C	T_{cc}/°C	T_c/°C	ΔH_c/J g^{-1}
PLA/10CeF 7.13	5	45.62	–	–	54.4	–	168.7	–	–	134.3	41.93
	10	43.31	–	–	51.7	–	167.6	–	–	127.4	40.9
	20	41.83	–	–	49.9	–	165.9	–	–	117.8	37.29
	40	37.19	–	3.47	40.2	164.8	168.8	–	92.0	100.5	25.80
PLA/20CeF 7.22	5	36.69	–	–	49.3	–	165.9	–	–	135.1	36.80
	10	36.97	–	–	49.6	–	167.4	–	–	128.5	36.40
	20	36.27	–	–	48.7	–	165.9	–	–	119.2	32.73
	40	32.35	–	1.51	41.4	164.4	169.2	–	91.8	103.9	24.90
PLA/30CeF 7.39	5	35.90	–	–	55.1	–	168.2	–	–	135.6	33.60
	10	34.28	–	–	52.6	–	167.6	–	–	129.2	32.02
	20	32.23	–	–	49.5	–	165.9	–	–	120.2	29.50
	40	29.20	–	0.31	44.3	164.2	169.4	–	90.8	105.9	23.79
PLA/10CeF$_P$ 5.41	5	43.91	–	–	52.4	–	167.8	–	–	133.6	40.70
	10	40.68	–	–	48.5	–	166.8	–	–	126.7	38.37
	20	35.65	0.48	5.66	35.2		164.1	151.3	93.0	117.0	35.39
	40	35.66	0.47	5.92	34.9	164.0	167.8	151.3	92.8	99.7	20.26
PLA/20CeF$_P$ 5.37	5	40.42	–	–	54.3	–	168.1	–	–	135.3	38.20
	10	38.11	–	–	51.2	–	166.9	–	–	128.8	35.71
	20	36.50	–	–	49.0	–	165.0	–	–	120.1	33.74
	40	33.61	–	–	45.1	163.9	169.1	–	–	105.1	26.23
PLA/30CeF$_P$ 5.19	5	36.43	–	–	55.9	–	168.0	–	–	136.7	34.10
	10	34.90	–	–	53.6	–	167.1	–	–	130.9	32.51
	20	31.81	–	–	48.8	–	165.8	–	–	122.7	31.40
	40	30.75	–	–	47.2	164.1	169.5	–	–	109.1	27.48
PLA/10CeF$_{O3}$ 6.43	5	38.18	–	–	45.6	–	166.6	–	–	136.2	34.22
	10	37.02	–	–	44.2	–	165.7	–	–	131.0	32.16
	20	35.40	–	–	42.2	–	164.2	–	–	123.4	30.78
	40	32.44	–	–	38.7	162.9	168.3	–	–	111.9	28.13
PLA/20CeF$_{O3}$ 7.38	5	44.87	–	–	60.2	–	168.1	–	–	135.7	39.92
	10	42.87	–	–	57.6	–	166.8	–	–	129.8	37.70
	20	41.10	–	–	55.2	–	165.2	–	–	122.0	36.81
	40	36.77	–	–	49.4	163.5	169.0	–	–	108.7	31.57
PLA/30CeF$_{O3}$ 7.12	5	40.15	–	–	61.6	–	167.6	–	–	135.9	36.01
	10	38.16	–	–	58.6	–	166.3	–	–	130.2	34.25
	20	36.94	–	–	56.7	–	165.1	–	–	122.6	32.70
	40	33.19	–	–	50.9	163.2	168.7	–	–	110.0	29.91
PLA-g-MAH/PLA/10CeF 7.12	5	50.11	–	–	60.1	–	168.3	–	–	134.7	45.33
	10	47.93	–	–	57.5	–	166.8	–	–	127.9	43.79
	20	46.01	–	–	55.2		165.6	–	–	118.9	40.27
	40	40.27	–	2.61	45.2	164.2	169.0	–	91.1	101.9	28.34
PLA-g-MAH/PLA/20CeF 6.77	5	40.52	–	–	54.7	–	168.4	–	–	135.0	36.94

Table 2 (continued)

Sample code and mass/mg	CR/°C min^{-1}	ΔH_m/J g^{-1}	ΔH_{pc}/J g^{-1}	ΔH_{cc}/J g^{-1}	χ_c/%	$T_{m\alpha}$/°C	$T_{m\alpha}$/°C	T_{pc}/°C	T_{cc}/°C	T_c/°C	ΔH_c/J g^{-1}
	10	37.89	–	–	51.2	–	167.3	–	–	128.3	35.35
	20	35.29	–	–	47.7	–	166.0	–	–	119.1	32.87
	40	31.49	–	0.96	41.2	164.3	169.6	–	91.0	103.9	25.14
PLA-g-MAH/PLA/30CeF 6.97	5	36.14	–	–	55.9	–	168.6	–	–	136.3	33.16
	10	34.48	–	–	53.3	–	167.4	–	–	130.2	31.79
	20	33.01	–	–	51.0	–	166.1	–	–	122.2	29.46
	40	29.97	–	–	46.3	164.2	169.4	–	–	108.6	25.56

CR: cooling rate; CeF_P: the plasma-treated surface of the cellulose fibres; CeF_{O3}: ozone-treated cellulose fibres surface

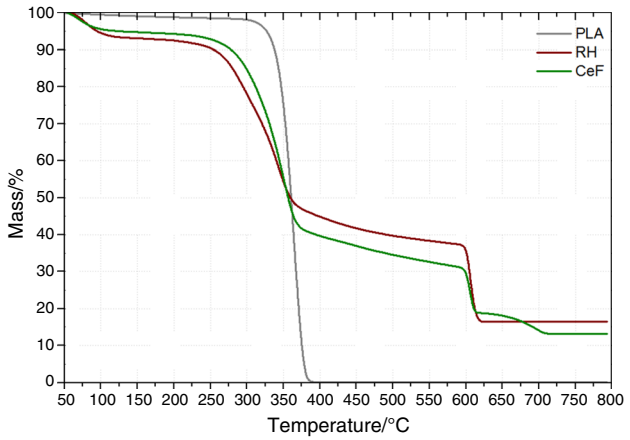

Fig. 6 Degree of PLA composites crystallinity with 10 mass% rice husk (RH) under different cooling rates

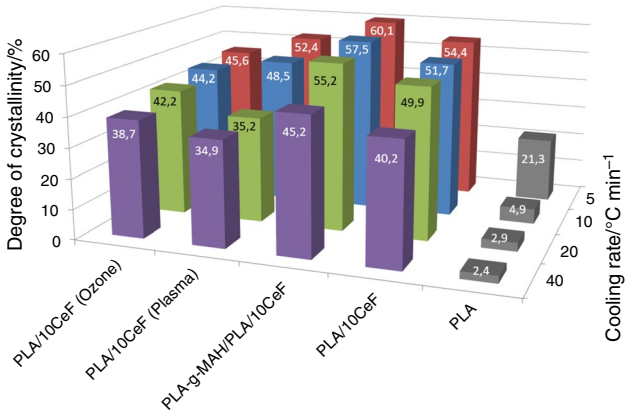

Fig. 7 Degree of PLA composites crystallinity with 10 mass% cellulose fibres (CeF) under different cooling rates

reached in low cooling rate markedly lower degree of crystallinity (Fig. 6). The influence of plasma and ozone surface treatments of RH, as well as the chemical treatment of PLA with maleic anhydride, on degree of crystallinity is for 20–30 mass% concentration insignificant. Contrariwise, the

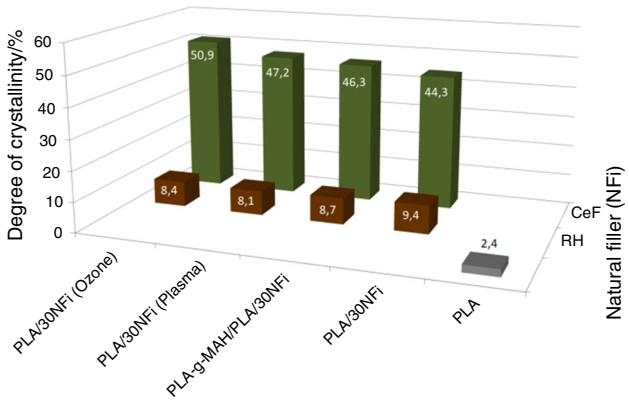

Fig. 8 Degree of PLA composites crystallinity with 30 mass% rice husks (RHs) or cellulose fibres (CeF) at cooling rate of 40 °C min^{-1}

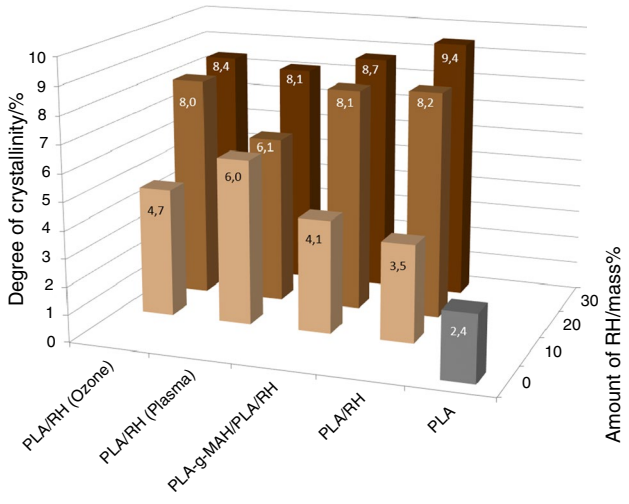

Fig. 9 Degree of PLA composites crystallinity with 10–30 mass% rice husks (RHs) at cooling rate of 40 °C min^{-1}

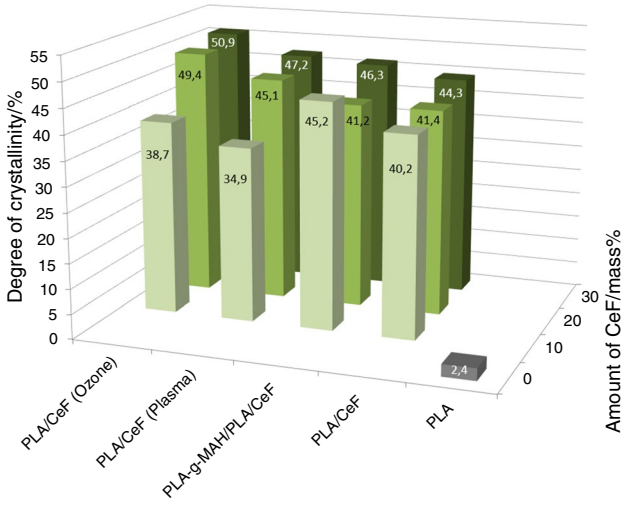

Fig. 10 Degree of PLA composites crystallinity with 10–30 mass% cellulose fibres (CeF) at cooling rate of 40 °C min^{-1}

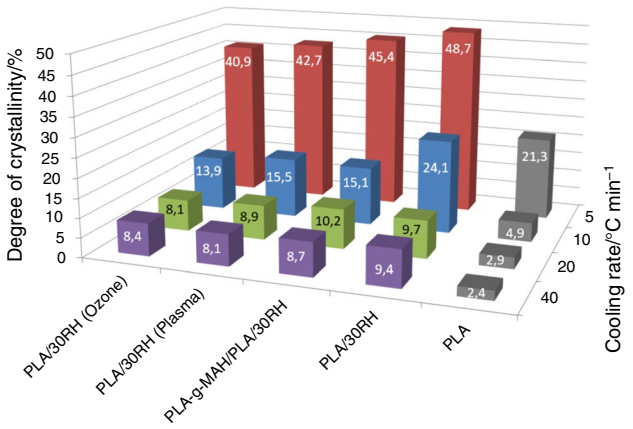

Fig. 11 Degree of crystallinity of PLA-based composites with 30 mass% rice husk (RH)

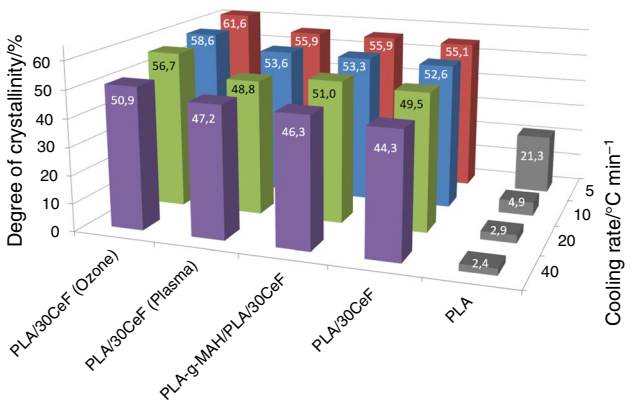

Fig. 12 Degree of PLA composites crystallinity with 30 mass% cellulose fibres (CeF) under different cooling rates

highest values were observed for RH composites without surface modification (Fig. 11).

Higher degree of crystallinity was observed for PLA composites with 10 mass% of CeF and grafted maleic anhydride onto macromolecule chain of PLA. The plasma and ozone surface treatment of CeF did not evoke any positive enhancements of degree of crystallinity (Fig. 7). Definitely, the highest degree of crystallinity was observed in PLA composites with 20–30 mass% of CeF which were treated with ozone (Fig. 12). Morphology changes and changes in chemical properties of fibres, evoked by ozone treatment, could be a reason of these enhancements. An influence of ozone treatment on changes of chemical properties of fibres was reported in research of Maqsood [38].

Non-isothermal crystallization kinetics

From the results of the relative crystallinity determination (Table 3), it can be seen that at T_c, the highest relative crystallinity at melt crystallization temperature (X_{Tc}) values is obtained for PLA composites with cellulose fibres. As can be seen in Fig. 13, these cellulose-based composites primarily crystallized at higher temperatures than those based on rice husks. The 20% and 30% increase in the peak relative crystallinity of PLA-g-MAH/PLA/10CeF compared to PLA-g-MAH/PLA/10RH composites has been observed at cooling rate (CR) of 5 and 10 °C min^{-1}, respectively. From obtained DSC data (Table 1 and Table 2) and traces of X_T–T curves (Fig. 13), it can be seen that fillers based on CeF show higher nucleation efficiency on PLA compared to RH-based fillers.

As it was already mentioned in the section of the absolute crystallinity degree evaluation, the plasma modification of the RH surface and the polymer structure modification by MAH grafting represent an important factor that affects the absolute degree of composite crystallinity, especially at a slow cooling rates and low filler content. From the graphical dependence on Fig. 14, it can be seen that with increasing cooling rates, a shorter time is required to reach the maximum value of the relative crystallinity degree. The higher retardation effect of cooling rate on the crystallization is observed at lower cooling rates. Furthermore, the obvious S shape of the X_T–t curve tends to straighten at a higher cooling rate. The same trends were observed by Zhou et al. [39] at PLLA-based systems. In addition, the plasma surface modification of RH caused a higher retardation effect on the PLA crystallization (Fig. 14) compared to PLA filled with neat RH and PLA-g-MAH/PLA/RH composites at both cooling rates (CR = 5 and CR = 10). With a higher cooling rate (CR = 10), it can be seen the negative effect of the plasma treatment and the modification of polymer structure by MAH on the crystallization time.

Table 3 Thermal analysis (DSC) data for the obtained PLA composites with ground rice husks (RHs) and cellulose fibres (CeF) inclusive determination of relative crystallinity at a peak melt crystallization temperature (X_{Tc})

CR/°C min^{-1}	Sample code and mass/mg	ΔH_{Tc}/J g^{-1}	X_{Tc}/%	Sample code and mass/mg	ΔH_{Tc}/J g^{-1}	X_{Tc}/%
5	PLA 5.53	6.08	47.8			
10		0.46	49.5			
20		–	–			
40		–	–			
5	PLA/10RH 6.99	3.80	48.3	PLA/10CeF 7.13	23.74	56.6
10		0.21	52.5		23.43	57.3
20		–	–		18.35	49.2
40		–	–		14.25	55.2
5	PLA/20RH 7.34	11.11	47.9	PLA/20CeF 7.22	20.18	54.8
10		1.47	49.2		19.05	52.3
20		–	–		18.61	56.9
40		–	–		12.99	52.2
5	PLA/30RH 6.96	13.59	52.8	PLA/30CeF 7.39	18.43	54.9
10		3.2	48.5		18.05	56.4
20		–	–		16.91	57.3
40		–	–		11.99	50.4
5	PLA/10RH$_P$ 5.79	9.53	46.4	PLA/10CeF$_P$ 5.41	22.26	54.7
10		0.75	46.3		21.82	56.9
20		–	–		18.89	53.4
40		–	–		10.59	52.3
5	PLA/20RH$_P$ 5.34	11.19	49.2	PLA/20CeF$_P$ 5.37	20.67	54.1
10		1.92	48.0		21.13	59.2
20		–	–		17.04	50.5
40		–	–		14.03	53.5
5	PLA/30RH$_P$ 5.73	10.77	50.0	PLA/30CeF$_P$ 5.19	18.45	54.1
10		1.98	51.3		18.73	57.6
20		–	–		17.92	57.1
40		–	–		13.70	49.9
5	PLA/10RH$_{O3}$ 5.69	6.1	44.6	PLA/10CeF$_{O3}$ 6.43	18.65	54.5
10		0.66	53.2		18.57	57.7
20		–	–		18.25	59.3
40		–	–		15.64	55.6
5	PLA/20RH$_{O3}$ 5.58	9.32	48.8	PLA/20CeF$_{O3}$ 7.38	20.94	52.5
10		1.58	50.2		21.91	58.1
20		–	–		20.45	55.6
40		–	–		16.54	52.4
5	PLA/30RH$_{O3}$ 6.09	9.17	47.0	PLA/30CeF$_{O3}$ 7.12	18.74	52.0
10		1.15	48.5		19.89	58.1
20		–	–		16.28	49.8
40		–	–		16.75	56.0

Table 3 (continued)

CR/°C min^{-1}	Sample code and mass/mg	ΔH_{Tc}/J g^{-1}	X_{Tc}/%	Sample code and mass/mg	ΔH_{Tc}/J g^{-1}	X_{Tc}/%
5	PLA-g-MAH/PLA/10RH 7.28	9.28	47.1	PLA-g-MAH/PLA/10CeF 7.12	25.95	57.2
10		0.67	44.4		25.18	57.5
20		–	–		19.71	48.9
40		–	–		13.69	48.3
5	PLA-g-MAH/PLA/20RH 7.40	11.52	48.4	PLA-g-MAH/PLA/20CeF 6.77	19.97	54.1
10		1.28	51.8		20.57	58.2
20		–	–		16.90	51.4
40		–	–		11.85	47.1
5	PLA-g-MAH/PLA/30RH 7.22	11.68	50.1	PLA-g-MAH/PLA/30CeF 6.97	19.01	57.3
10		1.44	48.8		18.67	58.7
20		–	–		16.58	56.3
40		–	–		11.44	44.8

CR: cooling rate; RH_P (CeF_P): the plasma-treated surface of the rice husks (cellulose fibres); RH_{O3} (CeF_{O3}): ozone-treated rice husk (cellulose fibres) surface

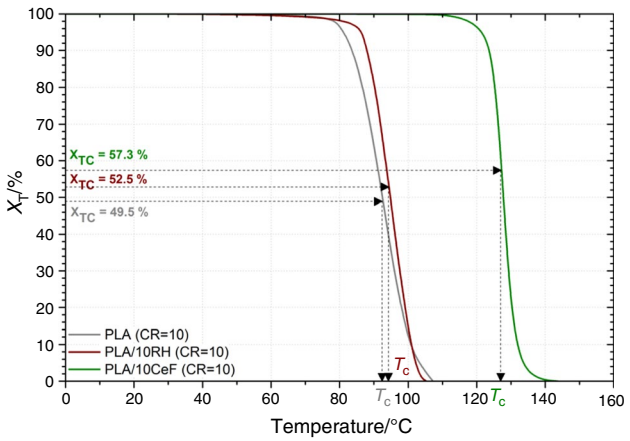

Fig. 13 Variation in X_T during the cooling rate (CR) of 10 °C min^{-1} for neat PLA, PLA/10RH and PLA/10CeF

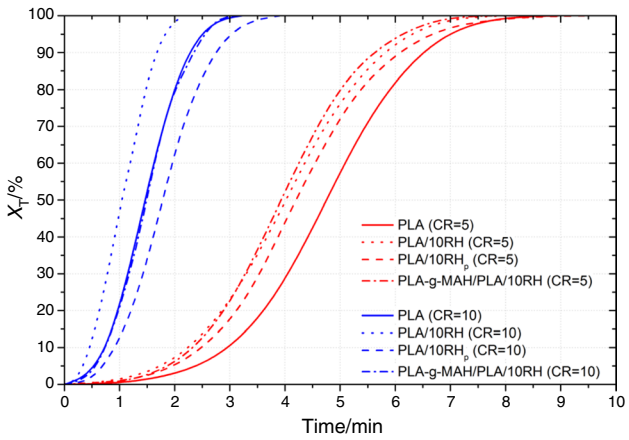

Fig. 14 Plots of relative degree of crystallinity as a function of time for neat PLA, PLA/10RH, PLA/10RH$_p$ and PLA-g-MAH/PLA/10RH at cooling rate (CR) of 5 °C min^{-1} and 10 °C min^{-1}

During the absolute degree of crystallinity evaluation of PLA/CeF composites, a positive influence of fibre surface treatment with ozone at a higher filler content (20–30 mass%) was found. In contrast, at a lower CeF loading (10 mass%) positive effect of MAH grafting was observed. Furthermore, in Fig. 15a it can be seen that surface treatment of CeF by ozonization accelerated the crystallization of PLA in contrast to neat CeF. However, this positive effect (as opposed to the total degree of crystallinity of the composite, see Table 2) can only be observed with decreasing cooling rate. At higher cooling rates, this otherwise positive effect of fibre surface modification on the crystallization rate of PLA tends to diminish. On the other hand, modification of polymer structure with MAH at low CeF loading (10 mass%) tends to fasten the crystallization at higher cooling rates (Fig. 15b).

Figure 16 shows the relative crystallinity degree evolution over the time plots for composite systems where the highest degree of absolute crystallinity (X_c) was recorded for both types of fillers (i.e. PLA/30CeF_{O3} and PLA/30RH). From the course of X_T–t curves, it is apparent that PLA composites with RH exhibit a higher retardation effect on the melt crystallization at both cooling rates. This retarding phenomenon tends to lower with increasing cooling rate. In contrast, PLA/30CeF_{O3} exhibits a faster transition to the glass region and X_T–t curve tends to straighten. Furthermore, unlike RH-based composites, there is no significant reduction in the

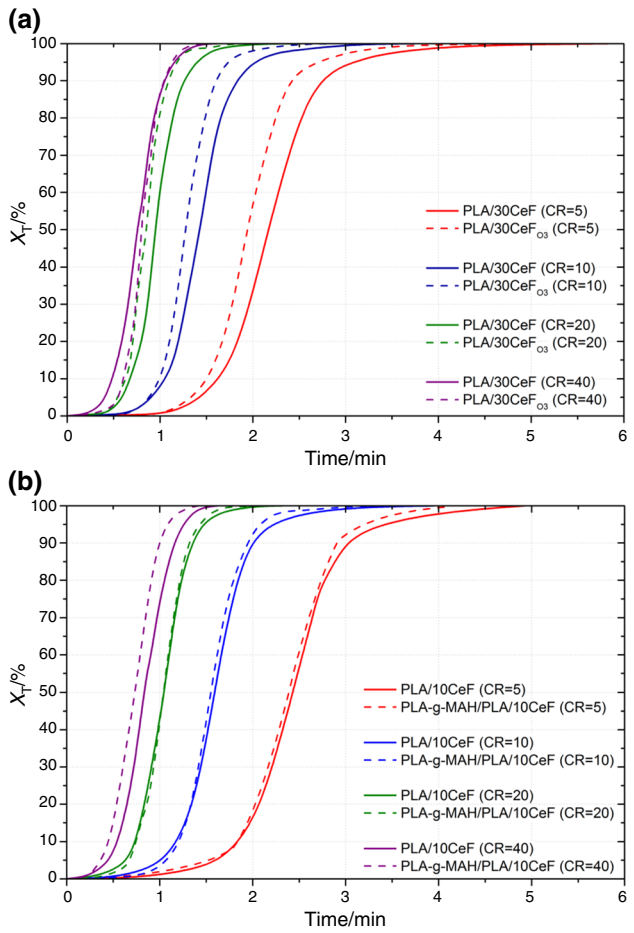

Fig. 15 Plots of relative degree of crystallinity as a function of time for **a** PLA/30CeF compared to PLA/30CeF$_{O3}$ and **b** PLA/10CeF compared to PLA-g-MAH/PLA/10CeF at all cooling rate (CR)

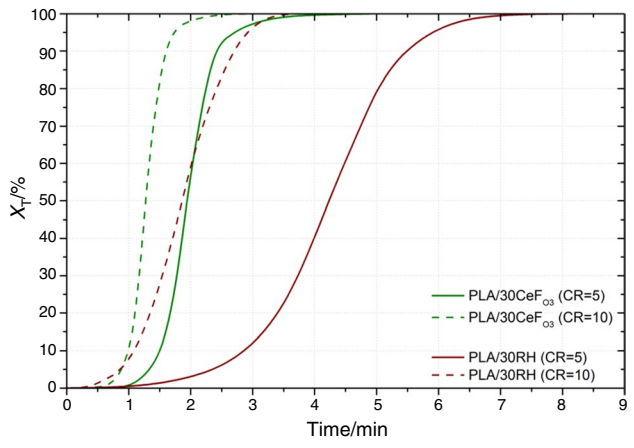

Fig. 16 Plots of relative degree of crystallinity as a function of time for PLA/30CeF$_{O3}$ compared PLA/30RH at cooling rate (CR) of 5 °C min^{-1} and 10 °C min^{-1}

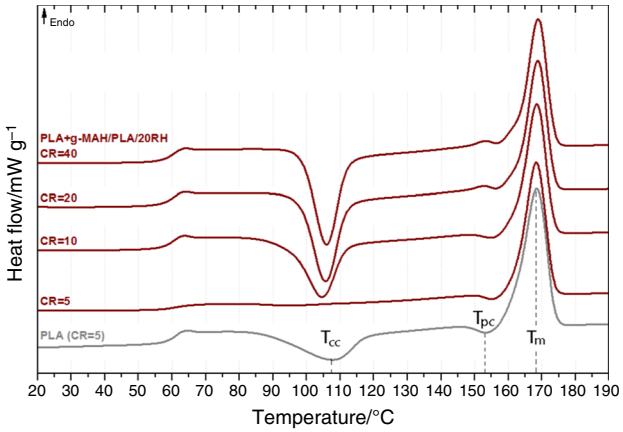

Fig. 17 DSC curves of PLA and PLA-g-MAH/PLA/20RH composites heating after previous cooling rate (CR)

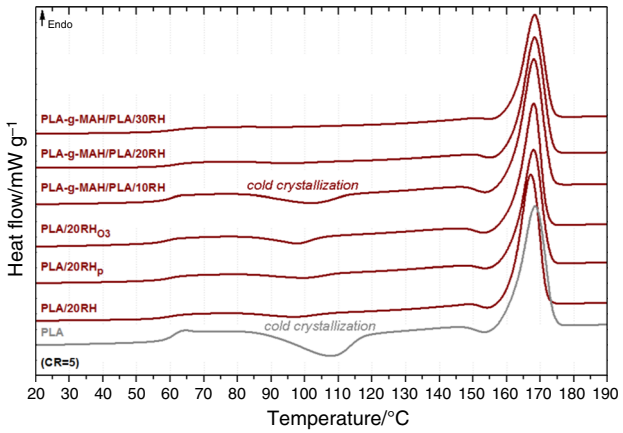

Fig. 18 DSC curves of PLA and PLA/RH composites after previous cooling rate (CR) of 5 °C min^{-1}

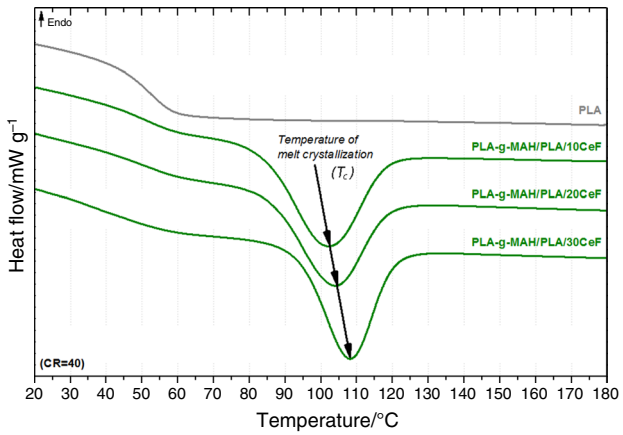

Fig. 19 Influence of CeF addition on melt crystallization temperature of PLA during cooling rate (CR) of 40 °C min^{-1}

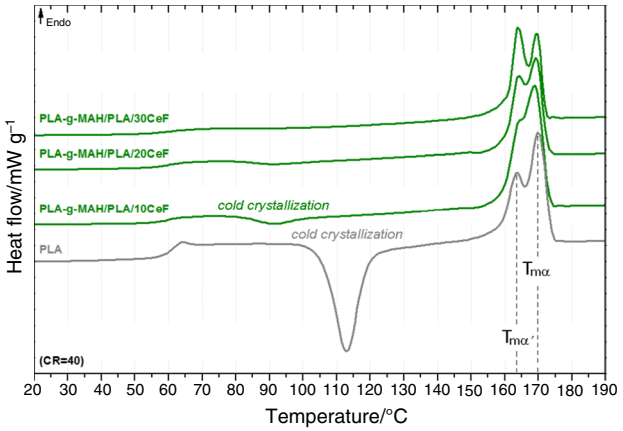

Fig. 20 Influence of CeF addition on cold crystallization of PLA after previous cooling rate (CR) of 40 °C min^{-1}

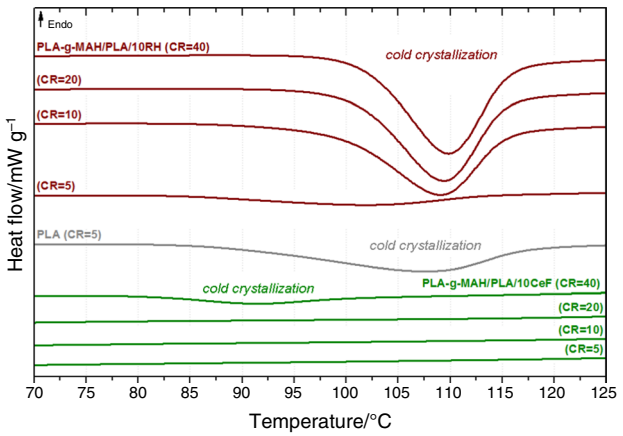

Fig. 21 Cold crystallization of PLA and PLA composites with 10 mass% RH and CeF after previous cooling rate (CR)

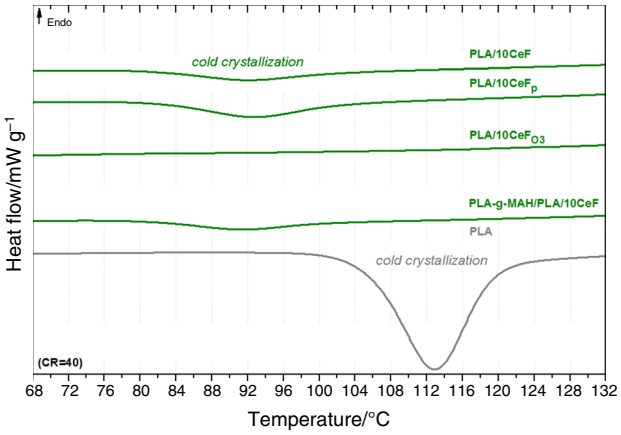

Fig. 22 Cold crystallization of PLA and PLA composites with 10 mass% CeF after previous cooling rate (CR) of 40 °C min^{-1}

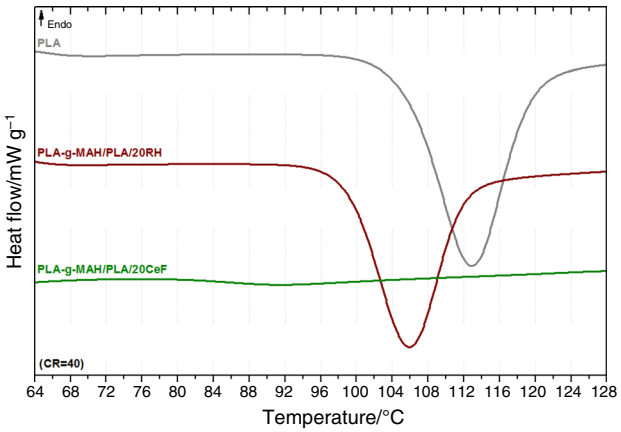

Fig. 23 Cold crystallization of PLA and PLA-g-MAH/PLA with 20RH and 20CeF after previous cooling rate (CR) of 40 °C min^{-1}

retarding effect in the measured cooling rate ranges. It is also evident from the graphs that the effect of cooling rate on the crystallization time of PLA is more significant for the RH-based fillers.

Cold and melt crystallization

As it was mentioned above, the poly(lactic acid) is in heating phase (temperature about 108–113 °C, depending on cooling rate) characteristic by its cold crystallization (Table 1). Cold crystallization is an exothermic crystallization process which is observed during heating of sample that has previously been cooled very quickly and has had no time to crystallize. Below the glass transition, molecular mobility is severely restricted and cold crystallization does not occur; above the glass transition, small crystallites are formed at relatively low temperatures. Cold crystallization temperature (T_{cc}) is increasing with cooling rate increase [22]. Heat of cold crystallization (ΔH_{cc}) is inversely proportional to the heat of melt crystallization (ΔH_c), as shown in Table 1. The evaluated results from DSC analysis declared that PLA significantly crystallizes from melt only by 5 and 10 °C min^{-1} cooling rate. The melt crystallization is not evident at higher cooling rates. Consequently, a considerable cold crystallization of PLA is observed. Comparable dependence is observed for PLA composites containing RH. Nevertheless, there is a difference in the level of heat of melt crystallization (Table 1). The heat of melt crystallization is for RH-based composites higher (Figs. 17 and 18). Further, the total elimination of cold crystallization was observed by slow cooling rate 5 °C min^{-1} of PLA composites containing 20–30 mass% of RH and grafted maleic anhydride (Fig. 18). For RH-based composites, the highest degree of crystallinity was observed in PLA-g-MAH/PLA composites which was cooled by rate 5 °C min^{-1}.

The introduction of cellulose fibres had during melt crystallization higher nucleation effect than RH. Significant shift of melt crystallization to higher temperatures even at high cooling rate (40 °C min^{-1}) has been noticed (Fig. 19). However, upon decrease in cooling rate any significant changes of melt crystallization temperatures have been observed (Table 2). Furthermore, more significant elimination of cold crystallization was noted by the presence of CeF contrary to the presence of RH in PLA composite (Table 2). For example, there was not observed any cold crystallization in composites PLA-g-MAH/PLA/CeF and PLA/CeF_p which contain the highest concentration of fibres (30 mass%) and where the highest cooling rate 40 °C min^{-1} was applied (Table 2 and Fig. 20.)

Contrary to RH, the initiation elimination of PLA cold crystallization was for CeF-based composites observed already at 10 mass% and cooling rates 5–20 °C min^{-1} (Fig. 21). The elimination of cold crystallization was for RH-based composited observed only at 5 °C min^{-1} cooling rate and 30 mass% in PLA matrix. The higher cooling rate 40 °C min^{-1} and low CeF amount caused elimination of cold crystallization only by ozone surface-treated composites (Fig. 22). From evaluated results, it is possible to state that increasing amount of CeF causes increase in degree of crystallinity and elimination of cold crystallization in PLA composites. Further, the ozone surface treatment of CeF has positive effect on degree of crystallinity and cold crystallization elimination. It is obvious especially by higher filler amount.

The rice husks and cellulose fibres have also influence on cold crystallization temperature of PLA. There was evaluated that with increasing amount of RH, the cold crystallization temperature of PLA decreases (in range of 7 to 10 °C). Cellulose fibres in PLA composite caused markedly decrease in cold crystallization or evoked its total elimination. At higher cooling rates (40 °C min^{-1}), temperature decrease about 21 °C was observed (Fig. 23).

Crystal polymorphism

Multiple melting peaks were observed in some DSC curves of PLA and PLA composites. There are differences in peaks which depend on varying cooling rates and different RH or CeF amounts. Multiple melting peaks indicate the presence of imperfect α′-crystals that have tendency to melt at lower temperatures ($T_{m\alpha'}$). The fast nucleation and consequently creation of imperfect α′-crystals, which are disordered crystals with the same conformation as the α-form but with loose packing, were observed under rapid cooling. Contrariwise, the α′-crystals generation was under increasing filler amount (RH, CeF) eliminated. There are several studies that investigate multiple melting peaks phenomenon of PLA [35, 40, 41]. These revealed that the phenomena of α′- and α-crystal formation can be correlated with crystallization condition. Furthermore, it was concluded that formation of α-crystals is replaced by formation of pseudohexagonal α′-crystals at temperatures lower than 120 °C [25]. Both forms can grow in temperature range from 100 to 120 °C, and at temperatures lower than 100 °C, only α′-crystals are made. The α′-crystals are metastable at the temperature of its formation, but transform into the stable α-form upon heating at their stability limit. Another event is the occurrence of exothermic peak at temperature T_{pc} (premelt crystallization). The exothermic peak reviled just before the melting peak. The reason could be transformation of disordered α′-crystals to more ordered α-crystals. There was observed exothermic premelt crystallization in PLA and PLA composites only when the low temperature of α′ was not detected (Table 1, Fig. 24).

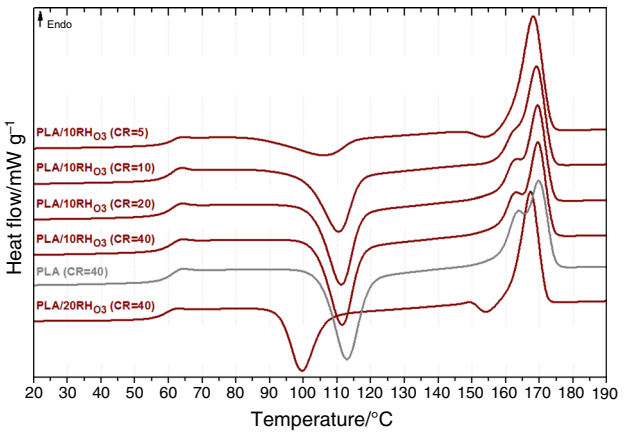

Fig. 24 DSC curves of PLA and PLA/10RH_{O3} composites heating after previous cooling rate (CR)

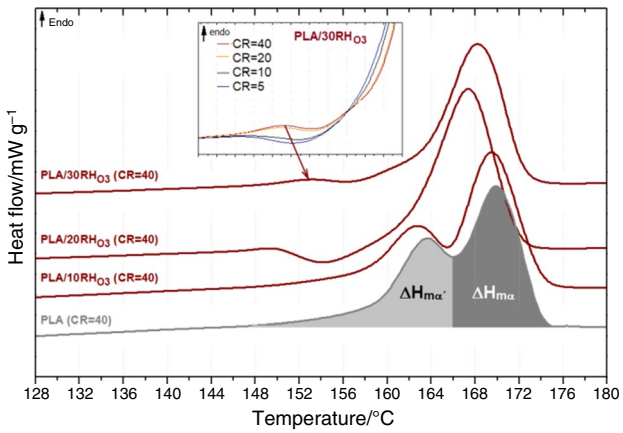

Fig. 25 The influence addition and amount of RH on α′-/α-polymorph transition of PLA after previous cooling rate (CR)

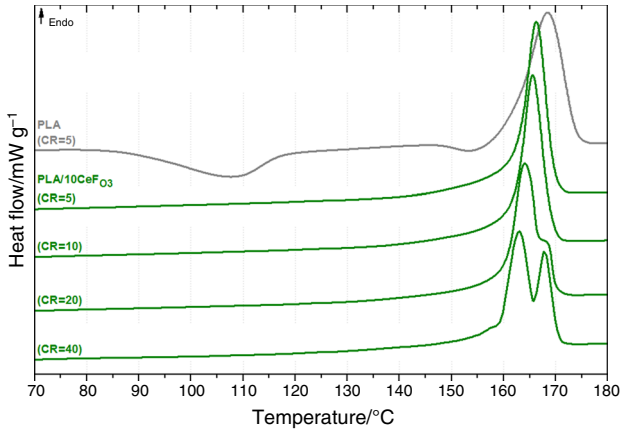

Fig. 26 DSC curves of PLA and PLA composites heating with 10 mass% CeF after previous cooling rate (CR)

The elimination of imperfect α′-crystals formation in PLA composites with 20–30 mass% by all applied cooling rates (5–40 °C min^{-1}) is obvious from our DSC results (Table 1). The DSC curves show an exotherm prior to the dominant melting peak, corresponding to the α′-to-α-crystalline phase transition (Fig. 24). The decreasing amount of imperfect α′-crystals was observed in composites where PLA-g-MAH was used within 10 mass% of RH. The comparable decrease was observed for plasma surface treatment of PLA composites containing the same amount of filler. The ratio of α′- and α-crystals is evaluated by heat of melting ($\Delta H_{m\alpha'}$ and $\Delta H_{m\alpha}$) which is corresponding to polymer mass% (Table 3 and Fig. 25).

In Fig. 25, the DSC curves of PLA composites, which contain α′-crystals and have different RH concentration, are shown. Multiple meting peaks were with the presence of RH eliminated. The small endothermic peak is observed around 153 °C in PLA composites with 20–30 mass% of RH. This evaluation corresponds with results study of Di Lorenzo and Androsch [23] where α′-/α-transitions under different heating rates were investigated. This endothermic peak is observed only at samples which undergoes previous higher cooling rates (Fig. 25). These phenomena can only be caused by melting of α′-crystals, which are further superimposed by exothermic formation of α-crystals and melt at a higher temperature. Regarding the evolution of the transition behaviour of RH composites, it is obvious that the exothermic reorganization event is outpaced by endothermic melting. This phenomenon is characteristic behaviour that occurs during heating of crystals with low thermal stability [23].

Contrariwise to RH, the cellulose fibres did not cause total elimination of imperfect α′-crystals of PLA in evaluated range of cooling rates (Fig. 26). While by composites containing 20–30 mass% of RH, the imperfect α′-crystals were eliminated at 40 °C min^{-1} cooling rate, the significant part of crystalline structure was composed of imperfect α′-crystals (evaluated from heat of melting $\Delta H_{m\alpha'}$) at cellulose-based composites of (Table 4).

Flexural modulus

Flexural modulus is material characteristic, which is significantly influenced by the morphology and crystallinity of polymers. In particular, heterogeneous structure of surface layers is important for high values of flexural modulus. In experimental measurement, there was observed flexural modulus increase with increasing RH and CeF amount. This statement is consistent with results research of Dimzoski et al. [42] and Graupner et al. [14]. Further, there were not observed any differences between RH and CeF at lower amount (10 mass%) of fillers. However, it was obvious that flexural modulus reached higher values at higher amount of CeF (20–30 mass%), as shown in Figs. 27–29. A positive effect of grafted maleic anhydride to stiffness increase was observed at lower amount (10 mass%) of RH. Nevertheless, it is important to state that the evaluated difference was low and that the influence of filler amount is at higher concentrations more considerable than any applied surface treatment. There was not observed any positive effect to flexural modulus enhancement at a variety of plasma surface treatment of CeF or grafted maleic anhydride (PLA-g-MAH/PLA/30CeF). The lowest effect on flexural modulus was noted at ozone-treated fillers.

Table 4 Heat of melting for α′- and α-crystals of PLA composites with rice husks (RHs) und cellulose fibres (CeF)

Sample code	CR/°C min^{-1}	$\Delta H_{m\alpha'}$/J g^{-1}	$\Delta H_{m\alpha}$/J g^{-1}	Sample code	CR/°C min^{-1}	$\Delta H_{m\alpha'}$/J g^{-1}	$\Delta H_{m\alpha}$/J g^{-1}
PLA 5.53	5	–	38.64				
	10	9.56	27.53				
	20	14.82	22.98				
	40	15.75	22.16				
PLA/10RH 6.99	5	–	32.31	PLA/10CeF 7.13	5	–	41.06
	10	10.05	22.48		10	–	38.98
	20	12.14	20.84		20	–	37.65
	40	12.56	20.44		40	11.01	22.46
PLA/20RH 7.34	5	–	27.73	PLA/20CeF 7.22	5	–	29.35
	10	–	27.31		10	–	29.58
	20	–	27.55		20	–	29.02
	40	–	27.61		40	12.54	13.34
PLA/30RH 6.96	5	–	22.20	PLA/30CeF 7.39	5	–	25.13
	10	–	22.58		10	–	24.00
	20	–	21.35		20	–	22.56
	40	–	21.48		40	11.31	9.13
PLA/10RH$_P$ 5.79	5	–	32.68	PLA/10CeF$_P$ 5.41	5	–	39.52
	10	4.54	26.58		10	–	36.61
	20	6.80	24.60		20	–	32.09
	40	7.57	23.77		40	9.41	22.69
PLA/20RH$_P$ 5.34	5	–	25.91	PLA/20CeF$_P$ 5.37	5	–	32.34
	10	–	25.45		10	–	30.49
	20	–	25.13		20	–	29.20
	40	–	25.03		40	13.83	13.06
PLA/30RH$_P$ 5.73	5	–	20.70	PLA/30CeF$_P$ 5.19	5	–	25.50
	10	–	20.59		10	–	24.43
	20	–	19.70		20	–	22.27
	40	–	16.61		40	13.55	7.97
PLA/10RH$_{O3}$ 5.69	5	–	32.27	PLA/10CeF$_{O3}$ 6.43	5	–	34.36
	10	10.36	20.39		10	–	33.32
	20	10.36	21.47		20	–	31.86
	40	10.58	20.75		40	18.89	10.31
PLA/20RH$_{O3}$ 5.58	5	–	25.31	PLA/20CeF$_{O3}$ 7.38	5	–	35.90
	10	–	24.94		10	–	34.30
	20	–	24.46		20	–	32.88
	40	–	24.51		40	17.14	12.28
PLA/30RH$_{O3}$ 6.09	5	–	20.43	PLA/30CeF$_{O3}$ 7.12	5	–	28.11
	10	–	19.82		10	–	26.71
	20	–	19.69		20	–	25.86
	40	–	19.72		40	14.18	9.06
PLA-g-MAH/PLA/10RH 7.28	5	–	32.73	PLA-g-MAH/PLA/10CeF 7.12	5	–	44.85

Table 4 (continued)

Sample code	CR/°C min^{-1}	$\Delta H_{m\alpha}$/J g^{-1}	$\Delta H_{m\alpha}$/J g^{-1}	Sample code	CR/°C min^{-1}	$\Delta H_{m\alpha}$/J g^{-1}	$\Delta H_{m\alpha}$/J g^{-1}
	10	4.51	26.77		10	–	42.90
	20	7.50	24.59		20	–	41.18
	40	7.93	23.62		40	11.56	24.48
PLA-g-MAH/PLA/20RH 7.40	5	–	26.78	PLA-g-MAH/PLA/20CeF 6.77	5	–	32.21
	10	–	26.31		10	–	30.12
	20	–	26.29		20	–	28.06
	40	–	26.41		40	11.45	13.59
PLA-g-MAH/PLA/30RH 7.22	5	–	20.57	PLA-g-MAH/PLA/30CeF 6.97	5	–	25.12
	10	–	20.68		10	–	23.96
	20	–	20.94		20	–	22.94
	40	–	20.95		40	12.59	8.24

CR: cooling rate; RH_P (CeF_P): the plasma-treated surface of the rice husks (cellulose fibres); RH_{O3} (CeF_{O3}): ozone-treated rice husk (cellulose fibres) surface

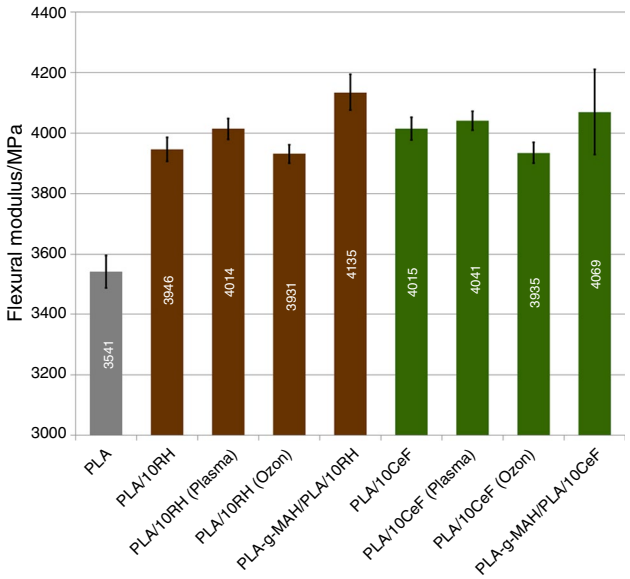

Fig. 27 Flexural modulus for PLA composites with 10 mass% RH and CeF

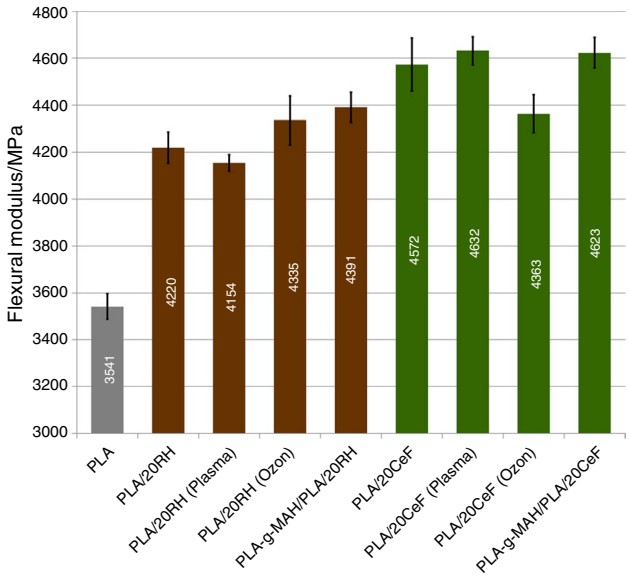

Fig. 28 Flexural modulus for PLA composites with 20 mass% RH and CeF

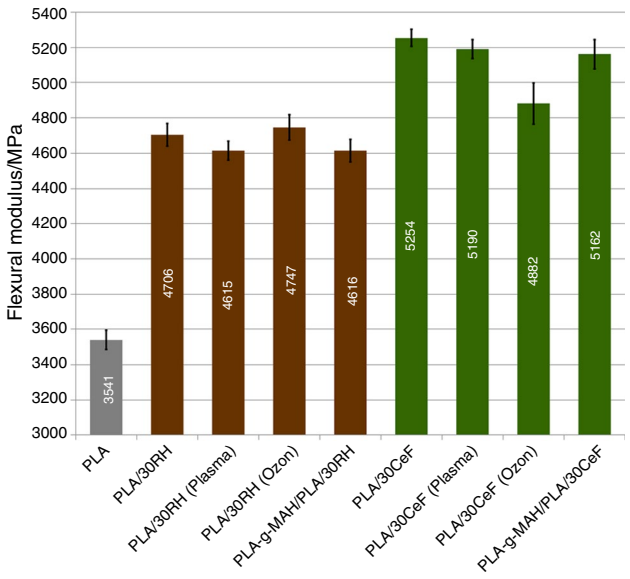

Fig. 29 Flexural modulus for PLA composites with 30 mass% RH and CeF

Conclusions

The presence of ground rice husks (RHs) and technical cellulose fibres (CeF) caused not only increase in stiffness of PLA composites but also enhanced crystallization kinetics. In PLA composites containing 30 mass% of RH, there was observed almost 32% increase in flexural modulus (4747 MPa), contrary to pure PLA (3541 MPa), and almost 48% increase (5224 MPa) in composites with the presence 30 mass% of CeF. Moreover, the lower filler amounts (10 mass%) evoked in PLA/RH and PLA/CeF composites a similar trend of flexural modulus increase. The influence of plasma and ozone surface treatment on stiffness was not observed. The positive effect of chemical treatment of grafted maleic anhydrides onto PLA matrix was evaluated only for PLA/RH composites with 10 mass% of fillers.

Consequently, a study of non-isothermal crystallization of RH- and CeF-based composites was performed. The influence of fillers amount, as well as physical surface treatment and chemical treatment based on compatibilizing agent introduction (PLA-g-MAH) under different cooling rates on thermal properties and crystallization kinetic, was investigated. A higher nucleation effect of CeF, which has average 13 mass% of $CaCO_3$, in PLA composites was observed, compared to the presence of RH in composites. Up to 20% and 30% increase in the peak relative crystallinity (X_{Tc}) of PLA-g-MAH/PLA/10CeF compared to PLA-g-MAH/PLA/10RH composites has been observed at cooling rate of 5 and 10 °C min^{-1}, respectively. The highest increase in absolute degree of crystallinity (compared to pure PLA) was noted in PLA/RH and PLA/CeF composites that were cooled by the highest rates. The highest increase was observed in CeF-based composites. The highest increase in absolute degree of crystallinity, by almost 4×, was observed in PLA composites containing 30 mass% of RH that was cooled by the highest cooling rate (40 °C min^{-1}) and almost 21× (from 2.4 into 51%) in PLA/CeF composites at the same amount of fillers. Further, the increase in absolute crystallinity degree with increasing amount of natural filler (especially RH) was noted. This is observed especially under intensive cooling rates. The increasing absolute degree of crystallinity with increasing amount of natural filler is not so significant for CeF as for RH. However, it is possible to state that the RH and CeF natural fillers eliminate the negative effect of cooling rate on PLA materials.

The positive influence of surface treatment of RH on absolute degree of crystallinity was noticeable only in PLA composites with 10 mass% of fillers. The highest absolute degree of crystallinity (33.5%) was reached in plasma surface-treated composites (from primary 17.9% in PLA/10RH and CR = 5). Comparable values of crystallinity degree of PLA-g-MAH composites (34.6%) were observed by slow cooling rate 5 °C min^{-1}. This positive effect was reached only at low cooling rate (CR = 5). With a higher cooling rates, an increase in crystallization time was observed. With increasing amount of RH, there was not evaluated any positive effect of surface treatments or grafted MAH for both determinations of absolute and relative degree of crystallinity. In addition, the plasma surface modification of RH caused a higher retardation effect on the PLA crystallization (Fig. 14) compared to PLA filled with neat RH and PLA-g-MAH/PLA/RH composites.

The composites with 10 mass% of CeF reached the highest absolute degree of crystallinity (60.1%) in variety of PLA with grafted MAH (from primary 54.4% in PLA/10CeF and CR = 5). A positive effect of surface-treated fibres was observed when ozone treatment of CeF with the amount up to 20–30 mass% was applied. Contrary to PLA-g-MAH composites (55.9%), even higher values of degree of crystallinity (61.6% in PLA/30CeF_{O3} and CR = 5) were observed for this formulation. Furthermore, surface treatment of CeF by ozonization accelerated the crystallization of PLA in contrast to neat CeF. This positive effect is more profound especially at lower cooling rates. On the other hand, modification of polymer structure with MAH at low CeF loading (10 mass%) tends to fasten the crystallization at higher cooling rates.

From the crystallization kinetics evaluation, it is apparent that PLA composites with RH exhibit a higher retardation effect on the melt crystallization. This retarding phenomenon tends to lower with increasing cooling rate. In contrast, PLA composites with CeF exhibit a higher nucleation efficiency and fastening of the crystallization kinetics.

Changes of degree of crystallinity, mentioned about, are reflection of melt crystallization kinetic. Its enhancements, due to the nucleation effect of RH and CeF, have significant influence on cold crystallization and crystal polymorphism of PLA. In experimental measurement, it was observed that the peak of meting crystallization temperature is moved to higher temperatures. The presence of CeF caused elimination of cold crystallization even in 10 mass% concentrations. The elimination of cold crystallization of composites was reached by cooling rates 5–20 °C min^{-1} and in composites containing ozone-modified CeF also by cooling rate 40 °C min^{-1}. Plasma surface treatment and PLA-g-MAH modification had an effect only in higher amounts of CeF (20 and 30 mass%). Contrary to CeF, the RH evoked the cold crystallization elimination of PLA only by slow cooling rates 5 °C min^{-1} and 30 mass% of filler. Further, the shift of cold crystallization temperatures to lower values was observed at presence of RH and CeF in PLA composites. The shift about 7–10 °C has been observed for composites with 30 mass% of RH. More intensive shift (about 21 °C) has been observed for composites with 30 mass% of CeF unless it was eliminated by slow cooling rate completely.

In evaluated thermal properties, the influence of RH and CeF on transformation behaviours of α′-/α-polymorphs was observed. The elimination of imperfect α′-crystals was observed with increasing amount of RH and CeF. The presence of RH and CeF in 20–30 mass% evoked elimination of α′-crystals creation in all cooling rate ranges (5–40 °C min^{-1}). The α′-crystals were in CeF composites eliminated already at 10 mass%, but only in cooling rate range 5–20 °C min^{-1}. Moreover, the endothermic event was observed in PLA/RH composites by cooling rate higher than 20 °C min^{-1}. This endothermic event was caused with melting of α′-crystals, which are then superimposed by exothermic formation of α-crystals that melt at a higher temperature. At the lower cooling rate, only α′-/α-exothermic transition is observed.

Acknowledgements This publication was written at the Technical University of Liberec as part of the project SGS 21280 "Research and development for innovation of materials and production technologies with application potential in mechanical engineering" with the support of the Specific University Research Grant, as provided by the Ministry of Education, Youth and Sports of the Czech Republic in the year 2019 and the European Union—European Structural and Investment Funds in the frames of Operational Programme Research, Development and Education—project Hybrid Materials for Hierarchical Structures (HyHi, Reg. No. CZ.02.1.01/0.0/0.0/16_019/0000843).

References

1. Thakur VK, Thakur MK, Kessler MR. Handbook of composites from renewable materials, Volume 1: structure and chemistry. 1st ed. Hoboken: Wiley; 2017.
2. Ebnesajjad S. Handbook of biopolymers and biodegradable plastics: properties, processing, and applications. 1st ed. Waltham, MA: Elsevier/William Andrew; 2013.
3. Xu H, Yang Y, Yu X. Lightweight materials from biopolymers and biofibers. 1st ed. Washington, DC: American Chemical Society; 2014.
4. Mohanty AK, Misra M, Drzal LT. Natural fibers, biopolymers, and biocomposites. 1st ed. Boca Raton: Taylor and Francis; 2005.
5. Dartora PC, da Rosa Loureiro M, de Camargo Forte MM. Crystallization kinetics and morphology of poly(lactic acid) with polysaccharide as nucleating agent. J Therm Anal Calorim. 2018. https://doi.org/10.1007/s10973-018-7744-3.
6. Prapruddivongs C, Rukrabiab J, Kulwongwit N, Wongpreedee T. Effect of surface-modified silica on the thermal and mechanical behaviors of poly(lactic acid) and chemically crosslinked poly(lactic acid) composites. J Thermoplast Compos Mater. 2019. https://doi.org/10.1177/0892705719835286.
7. Jia S, Yu D, Zhu Y, Wang Z, Chen L, Fu L. Morphology, crystallization and thermal behaviors of PLA-based composites: wonderful effects of hybrid GO/PEG via dynamic impregnating. Polymers. 2017. https://doi.org/10.3390/polym9100528.
8. Fang Q, Hanna MA. Rheological properties of amorphous and semicrystalline polylactic acid polymers. Ind Crops Prod. 1999. https://doi.org/10.1016/S0926-6690(99)00009-6.
9. Ding W, Chu RK, Mark LH, Park CB, Sain M. Non-isothermal crystallization behaviors of poly(lactic acid)/cellulose nanofiber composites in the presence of CO_2. Eur Polym J. 2015. https://doi.org/10.1016/j.eurpolymj.2015.07.054.
10. Hamdan MHM, Siregar JP, Rejab MRM, Bachtiar D, Jamiluddin J, Tezara C. Effect of maleated anhydride on mechanical properties of rice husk filler reinforced PLA matrix polymer composite. Int J Precis Eng Manuf-Green Technol. 2019. https://doi.org/10.1007/s40684-019-00017-4.
11. Haylock R, Rosentrater KA. Cradle-to-grave life cycle assessment and techno-economic analysis of polylactic acid composites with traditional and bio-based fillers. J Polym Environ. 2018. https://doi.org/10.1007/s10924-017-1041-2.
12. Li Y, Han C, Yu Y, Xiao L, Shao Y. Effect of content and particle size of talc on nonisothermal melt crystallization behavior of poly(L-lactide). J Therm Anal Calorim. 2019. https://doi.org/10.1007/s10973-018-7365-x.
13. Greco A, Ferrari F, Maffezzoli A. Thermal analysis of poly(lactic acid) plasticized by cardanol derivatives. J Therm Anal Calorim. 2018. https://doi.org/10.1007/s10973-018-7059-4.
14. Graupner N, Herrmann AS, Müssig J. Natural and man-made cellulose fibre-reinforced poly(lactic acid) (PLA) composites: an overview about mechanical characteristics and application areas. Compos A Appl Sci Manuf. 2009. https://doi.org/10.1016/j.compositesa.2009.04.003.
15. Murariu M, Dubois P. PLA composites: from production to properties. Adv Drug Deliv Rev. 2016. https://doi.org/10.1016/j.addr.2016.04.003.
16. Thakur VK, Singha AS. Surface modification of biopolymers. 1st ed. Hoboken: Wiley; 2015.
17. Kalia S, Thakur K, Celli A, Kiechel MA, Schauer CL. Surface modification of plant fibers using environment friendly methods for their application in polymer composites, textile industry and antimicrobial activities: a review. J Environ Chem Eng. 2013. https://doi.org/10.1016/j.jece.2013.04.009.

18. Jang JY, Jeong TK, Oh HJ, Youn JR, Song YS. Thermal stability and flammability of coconut fiber reinforced poly(lactic acid) composites. Compos Part B Eng. 2012. https://doi.org/10.1016/j.compositesb.2011.11.003.
19. Tran TPT, Bénézet JC, Bergeret A. Rice and Einkorn wheat husks reinforced poly(lactic acid) (PLA) biocomposites: effects of alkaline and silane surface treatments of husks. Ind Crops Prod. 2014. https://doi.org/10.1016/j.indcrop.2014.04.012.
20. Bourmaud A, Pimbert S. Investigations on mechanical properties of poly(propylene) and poly(lactic acid) reinforced by miscanthus fibers. Compos Part Appl Sci Manuf. 2008. https://doi.org/10.1016/j.compositesa.2008.05.023.
21. Mazzanti V, Pariante R, Bonanno A, Ballesteros OR, Mollica F, Filippone G. Reinforcing mechanisms of natural fibers in green composites: role of fibers morphology in a PLA/hemp model system. Compos Sci Technol. 2019. https://doi.org/10.1016/j.compscitech.2019.05.015.
22. Di Lorenzo ML, Androsch R. Synthesis, structure and properties of poly(lactic acid). 1st ed. New York: Springer; 2017.
23. Di Lorenzo ML, Androsch R. Influence of α′-/α-crystal polymorphism on properties of poly(L-lactic acid). Polym Int. 2019. https://doi.org/10.1002/pi.5707.
24. Zhang C, Lan Q, Zhai T, Nie S, Luo J, Yan W. Melt crystallization behavior and crystalline morphology of polylactide/poly(ε-caprolactone) blends compatibilized by lactide-caprolactone copolymer. Polymers. 2018. https://doi.org/10.3390/polym10111181.
25. Nagarajan V, Zhang K, Misra M, Mohanty AK. Overcoming the fundamental challenges in improving the impact strength and crystallinity of PLA biocomposites: influence of nucleating agent and mold temperature. ACS Appl Mater Interfaces. 2015. https://doi.org/10.1021/acsami.5b01145.
26. Arjmandi R, Hassan A, Majeed K, Zakaria Z. Rice husk filled polymer composites. Int Polym Sci. 2015. https://doi.org/10.1155/2015/501471.
27. Cortés JD, Carriazo JG, Sierra CA, Ochoa-Puentes C. Microcomposites based on polylactic acid with kaolinite or rice husk particles and their performance on water vapor permeability. J Macromol Sci Part A. 2017. https://doi.org/10.1080/10601325.2017.1317580.
28. Chandrasekhar S, Satayanarayana KG, Pramada PN, Raghavan P, Gupta TN. Review processing, properties and applications of reactive silica from rice husk—an overview. J Mater Sci. 2003. https://doi.org/10.1023/A:1025157114800.
29. Wen X, Zhang K, Wang Y, Han L, Han C, Zhang H, Chen S, Dong L. Study of the thermal stabilization mechanism of biodegradable poly(L-lactide)/silica nanocomposites. Polym Int. 2010. https://doi.org/10.1002/pi.2927.
30. Zhang J, Lou J, Ilias S, Krischnamachari P, Yan J. Thermal properties of poly(lactic acid) fumed silica nanocomposites: experiments and molecular dynamics simulations. Polymer. 2008. https://doi.org/10.1016/j.polymer.2008.02.048.
31. Data sheet Arbocel ZZC 500.
32. Peters F, Hünnekens B, Wieneke S, Militz H, Ohms G, Viöl W. Corrigendum: comparison of three dielectric barrier discharges regarding their physical characteristics and influence on the adhesion properties on maple, high density fiberboards and wood plastic composite. J Phys D Appl Phys. 2017. https://doi.org/10.1088/1361-6463/aab378.
33. Battegazzore D, Bocchini S, Alongi J, Frache A. Rice husk as biosource of silica: preparation and characterization of PLA–silica bio-composites. RSC Adv. 2014. https://doi.org/10.1039/C4RA05991C.
34. Reig FB, Adelantado JVG, Moreno MCMM. FTIR quantitative analysis of calcium carbonate (calcite) and silica (quartz) mixtures using the constant ratio method. Application to geological samples. Talanta. 2002. https://doi.org/10.1016/S0039-9140(02)00372-7.
35. Zhang J, Tashiro K, Tsuji H, Domb AJ. Disorder-to-order phase transition and multiple melting behavior of poly(L-lactide) investigated by simultaneous measurements of WAXD and DSC. Macromolecules. 2008. https://doi.org/10.1021/ma0706071.
36. Saeidlou S, Huneault MA, Li H, Park CB. Poly(lactic acid) crystallization. Prog Polym Sci. 2012. https://doi.org/10.1016/j.progpolymsci.2012.07.005.
37. Eiras DP, Pessan LA. Influence of calcium carbonate nanoparticles on the crystallization of polypropylene. Mater Res. 2009. https://doi.org/10.1590/S1516-14392009000400024.
38. Maqsood HS. Cellulose micro/nano particles from jute. Liberec: TU of Liberec; 2016.
39. Zhou WY, et al. Isothermal and non-isothermal crystallization kinetics of poly(L-lactide)/carbonated hydroxyapatite nanocomposite microspheres. In: Reddy B, editor. Advances in diverse industrial applications of nanocomposites. Rijeka: InTech Europe; 2001. p. 231–60.
40. Di Lorenzo ML. Crystallization behavior of poly(L-lactic acid). Eur Polym J. 2005. https://doi.org/10.1016/j.eurpolymj.2004.10.020.
41. Sarasua JR, Prud'homme RE, Wisniewski M, Le Borgne A, Spassky N. Crystallization and melting behavior of polylactides. Macromolecules. 1998. https://doi.org/10.1021/ma971545p.
42. Dimzoski S, Bogoeva-Gaceva G, Gentile G, Avelle M, Errico ME, Srebrenkoska V. Preparation and characterization of poly(lactic acid)/rice hulls based biodegradable composites. J Polym Eng. 2008;28:369–83.